



UKAEA

Preprint



MAGNETIC ISLANDS AND DISRUPTIONS IN A TOKAMAK

D C ROBINSON
K McGUIRE

CULHAM LABORATORY
Abingdon Oxfordshire

1979

This document is intended for publication in a journal or at a conference and is made available on the understanding that extracts or references will not be published prior to publication of the original, without the consent of the authors.

Enquiries about copyright and reproduction should be addressed to the Librarian, UKAEA, Culham Laboratory, Abingdon, Oxfordshire, England

MAGNETIC ISLANDS AND DISRUPTIONS IN A TOKAMAK

D. C. Robinson and K. McGuire[†]

Culham Laboratory, Abingdon, Oxon. OX14 3DB, U.K.
(Euratom/UKAEA Fusion Association)

ABSTRACT

Measurements with a magnetic probe, internal coils, soft x-rays and visible light on a small tokamak reveal the presence of tearing modes with $m = 4, 3, 2$ and $n = 1$. The modes grow, rotate and saturate at a level $b_r/B_\theta \lesssim 3\%$ which gives rise to magnetic islands of width ≈ 1.5 cm for $m = 3$. The islands are more elongated at this level than a simple calculation suggests and field line calculations and experiments suggest that the surfaces may be broken between them. The island width is predicted using a cylindrical initial value calculation for the instabilities using the measured current distribution, saturation level and magnetic Reynolds number. If the $m = 3$ mode exceeds the 3% level a minor disruption results. An $m = 2$ mode at a level of 6% gives rise to a major disruption whether or not an internal $m = 1$ mode is present. No other mode appears to play a significant role in the disruptive process.

[†]University of Oxford

(Submitted for publication in Nuclear Fusion).

August 1978

Magnetic field measurements have been made in the outer regions of a small multipole tokamak, TOSCA [1], whose parameters are shown in Table 1, major radius 30 cm, plasma radius ≤ 8.5 cm. There is no conducting shell. A conducting vacuum vessel, $r_v = 10$ cm with penetration time $7 \mu s$, is surrounded by 16 equally spaced single turn coils. They induce the plasma current and provide shaping fields. Equilibrium is maintained by a separate vertical field winding. A probe consisting of 24 coils 4 mm apart is used to measure simultaneously the radial, poloidal and toroidal fields. The frequency response of the coils is ≤ 5 MHz. The probe is enclosed in a quartz envelope 6 mm in diameter. Damage to the probe is avoided by making measurements only in discharges which have no runaway component as measured with a soft X-ray detector (SiLi 1-50 keV). The probe can be inserted 5 cm into the plasma vertically without affecting the conductivity temperature (~ 30 eV for these measurements) or the magnetic oscillations measured with external coils. The current distribution is affected slightly by the probe, which causes it to contract by a few mm. External coils, 16 poloidally, 8 toroidally, sin/cos coils and multipole moment coils [2] are used to monitor external magnetic field perturbations. Surface barrier detectors positioned both poloidally and toroidally monitor soft x-ray perturbations ($E \geq 0.6$ keV) at radii up to 5 cm.

Figure 1 shows the poloidal field from the inserted probe at radii of 6.2 and 7.4 cm. Apart from the regular oscillations the fluctuation level $\delta B_\theta / B_\theta$ is $< 1\%$. The oscillations $500 \mu s$ after the start of the plasma current (marked by the arrow on the figure) are deduced to be associated with an $m = 3, n = 1$ mode, where m, n are the poloidal and toroidal mode numbers respectively. The radial and poloidal field components are out of phase as are the two oscillating poloidal field components in the figure. The oscillating toroidal field component is observed to be an order of magnitude smaller. Later an $m = 2, n = 1$ mode appears (at $800 \mu s$ in Figure 1) when the current distribution has contracted before ultimately disrupting in this case.

High frequency fluctuations at 100 - 400 kHz with $b_r/B_\theta \approx 0.1\%$ are observed, superimposed on the low frequency oscillations. These appear to have a cross field correlation length of ~ 1 cm. Figure 2 shows the radial distribution of the $m = 3$ oscillating radial and poloidal field components and the arrow indicates the position of the surface where q , the safety factor, is equal to 3. The external coils show that the $m = 3$ perturbation is rotating in the direction of electron diamagnetic drift. The measured frequency would correspond to an electron temperature of 30 eV at the $q = 3$ surface. However a significant radial electric field is measured to be present with a probe. The amplitude of the radial magnetic field component reaches a maximum of about 3% of the peak poloidal field. Earlier in time an $m = 4$ perturbation with a somewhat smaller amplitude is often seen. The maximum radial field whose time rate of change is shown in Figure 3, is observed not to be sinusoidal in character though the higher harmonics are reduced near the vacuum vessel wall (the frequency is limited to less than 100 kHz in this figure). Soft X-ray measurements show a similar non-sinusoidal behaviour for $m = 2$. The evolution of the current distribution for this type of discharge is indicated in Figure 4 by a plot of the measured current density at 6.8 cm compared with the average current. Initially the current distribution is peaked when a magnetic aperture formed by the primary windings and the applied vertical field exists. The distribution then expands and becomes more uniform at 300 μ s when the $m = 4$ and 3 modes are excited from a rational surface where the current gradient is observed to be large. From 400 μ s the current distribution contracts until a disruption occurs in this case at 1 ms. This contraction is a result of too rapid a rise in density, producing a thermal instability.

If the $m = 3$ mode increases in amplitude above about 3% then the spikes as seen in Figure 3 increase in amplitude and the plasma performs a minor disruption i.e. the current density is observed to broaden in less than 10 μ s.

The extrapolated q value in the centre is greater than unity. The plasma always recovers from these minor disruptions. When the $m = 2$ mode increases in a similar way a single large positive going spike on the poloidal field is produced as indicated by the arrow in Figure 5, with a rise time of less than $10 \mu\text{s}$. Figure 5 shows the poloidal field at 4.6 and 5.7 cm. The peaked current distribution is flattened and the characteristic negative voltage spike and increase in plasma current associated with the rapid decrease in plasma inductance are observed. The $m = 2$ mode is observed to grow exponentially before the disruption, the external coils and soft X-ray measurements show that no other mode is present in this case. The time scale is some twenty times slower than the poloidal Alfvén transit time ($\frac{1}{2} \mu\text{s}$). The magnetic Reynolds number with respect to the poloidal field is $S_\theta \sim 3000$ and with respect to the toroidal field $\sim 36,000$. Evidently the phenomena is proceeding on a resistive instability timescale as measurements on varying the poloidal field show. We have no explanation for the "poloidal field spike" on the basis of a simple Ohms law. The spike is not observed outside the current carrying column.

Resistive instabilities in cylindrical geometry are predicted using an initial value calculation [3] with the measured current distribution and experimental parameters, S , when an $m = 3$ mode is observed. Figure 6 shows the computed radial and poloidal fields for a tearing mode. This is very similar to that observed in the experiment - Figure 2. The predicted growth time is $\sim 60 \mu\text{s}$ which is comparable to that observed, though the inclusion of toroidal and finite larmor radius effects may alter this value. Using computed radial field perturbations with varying amplitude results in the flux contours shown in Figure 7. The magnetic islands produced have a width of up to 2.0 cm for a 3% amplitude. This is comparable to that predicted using $w = 4 \left(\frac{b}{B_\theta} \frac{r}{m} \frac{q}{dq/dr} \right)^{\frac{1}{2}}$ and with that predicted by non-linear calculations [4].

This saturation width is about four times the resistive layer thickness obtained from the linearised calculation with the experimental value for the magnetic Reynolds number. The ion larmor radius is about 2 mm. The experimental situation is more complicated, the non-sinusoidal character shows that the magnetic islands are more elongated than shown in Figure 7(a) or (b) and Figure 7(c) shows an interpretation of the islands based upon the non-sinusoidal behaviour. The surfaces may be broken between the islands. This is confirmed by the correlation between X-ray emission from a soft runaway component (≤ 4 keV) and the peak amplitude of the mode. A Langmuir probe positioned at a radius greater than that of the limiter also shows a strong correlation with the peak amplitude of the mode. The breakage may be due to toroidal effects [5], but field line calculations for the device show that it may be due to small error fields associated with the primary windings.

The $m = 2$ magnetic islands calculated in the same way are shown in Figure 8. For an amplitude of $\approx 2\%$ soft X-ray measurements show that the temperature is affected by the presence of the mode. At a slightly higher amplitude the cooling can be detected on the diamagnetic loop. The island width tends to 3.0 cm just before disruption which occurs with $q(0) > 1$ ($q(0) \sim 1.4$ being typical). This is supported by the observation that for this type of discharge no sawtooth oscillations are observed on the soft X-ray detectors. Other discharges at lower density do exhibit sawtooth oscillations [6] but with reduced or no $m = 2$ activity. Figure 8 shows that the central surfaces bifurcate at about the amplitude associated with disruption (6%). The structure of the $m = 2$ islands as investigated elsewhere [6,7] is confirmed by radial scans with fibre guides and interference filters monitoring oscillations on line radiation from the plasma. The observations of the minor and major disruption fit quite closely with

the non-linear tearing mode calculations of White et al^[8]. Note that this device possesses a point limiter in the outer horizontal plane, the mode structure at disruption appears to be uncorrelated with contact on this limiter. This was also confirmed using a triangular plasma controlled by a separatrix^[9].

It is concluded that $m = 4, 3$ and 2 , $n = 1$ tearing modes are produced in this tokamak by the current gradient. The $m = 3$ mode saturates at an amplitude of $b_r/B_\theta \leq 3\%$ with a corresponding island width of ≤ 2.0 cm. At or above this level surface destruction and a minor disruption occurs. The $m = 2$ islands reach 3.0 cm in size before a major disruption occurs and no other mode is observed to be present in the disruptive process on this device.

We would like to thank J. A. Fessey for his careful construction of the magnetic probe and A. J. Wootton for discussions.

REFERENCES

- [1] G. Cima et al in Plasma Physics and Controlled Nuclear Fusion Research. (Proc. 6th Int. Conf. Berchtesgaden 1976) I.A.E.A., Vienna. 1(1977) 335.
- [2] L.E. Zakharov, V.D. Shafranov. Nuclear Fusion 11, (1971) 605.
- [3] J.E. Crow et al. Proc. 6th European Conf. on Controlled Fusion and Plasma Physics. Moscow 1, (1973) 567.
- [4] R.B. White et al. Phys. Fluids 20, (1977) 800.
- [5] J.M. Finn, Nuclear Fusion 15, (1975) 845.
- [6] S. von Goeler, 7th European Conf. on Controlled Fusion and Plasma Physics. Lausanne 2, (1975) 71.
- [7] H. Toyama, Plasma Physics and Controlled Nuclear Fusion Research. (Proc. 6th Int. Conf. Berchtesgaden 1976) I.A.E.A., Vienna 1(1977) 323.
- [8] R.B. White et al. Phys. Rev. Letters 39, (1977) 1618.
- [9] K. McGuire et al. Plasma Physics and Controlled Nuclear Fusion Research. 7th Int. Conf., Innsbruck, 1978 Paper CN/37 T-1/1.

Table 1 TOSCA PARAMETERS

R_p	30 cm
a_p	≤ 8.5 cm
I_p	10 - 15 kA
B_ϕ	0.4T - 0.6T
β_I	0.3 - 0.8
$\frac{1}{2a} \int n_e dl$	$1 - 4 \times 10^{13} \text{ cm}^{-3}$
$T_e(0)$	100 - 300 eV
τ_E	0.2 - 1.0 ms
V	1.5 → 4 volts

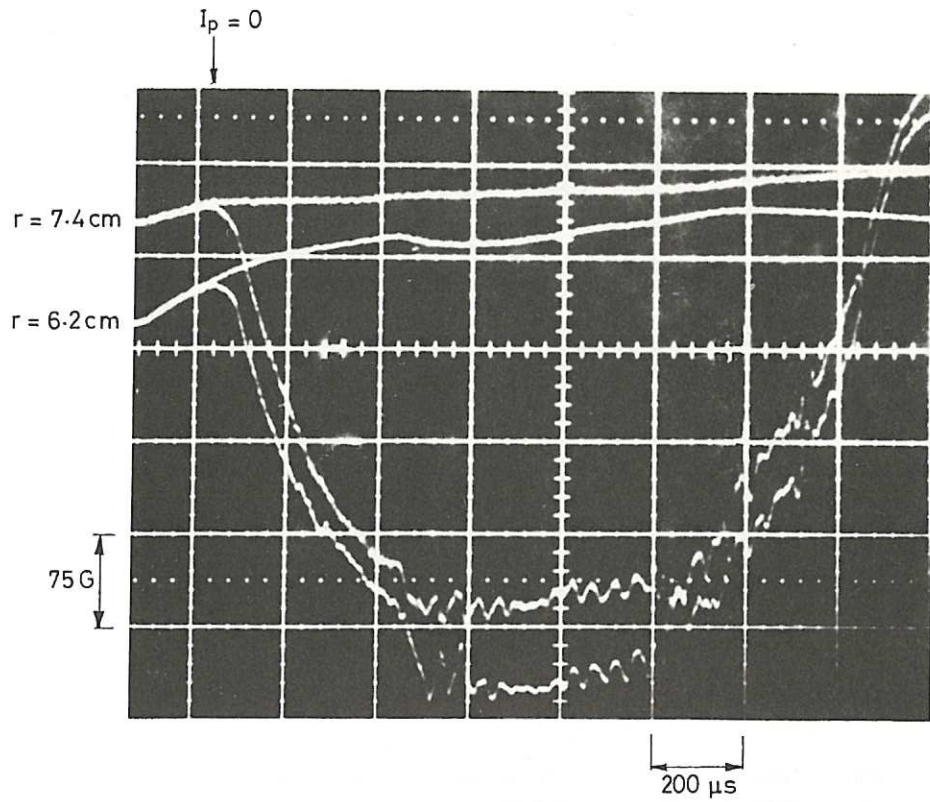


Fig. 1 Poloidal fields measured at radii of 7.4 and 6.2 cm respectively. Vertical scale 75 G/division, horizontal 200 μs /division.

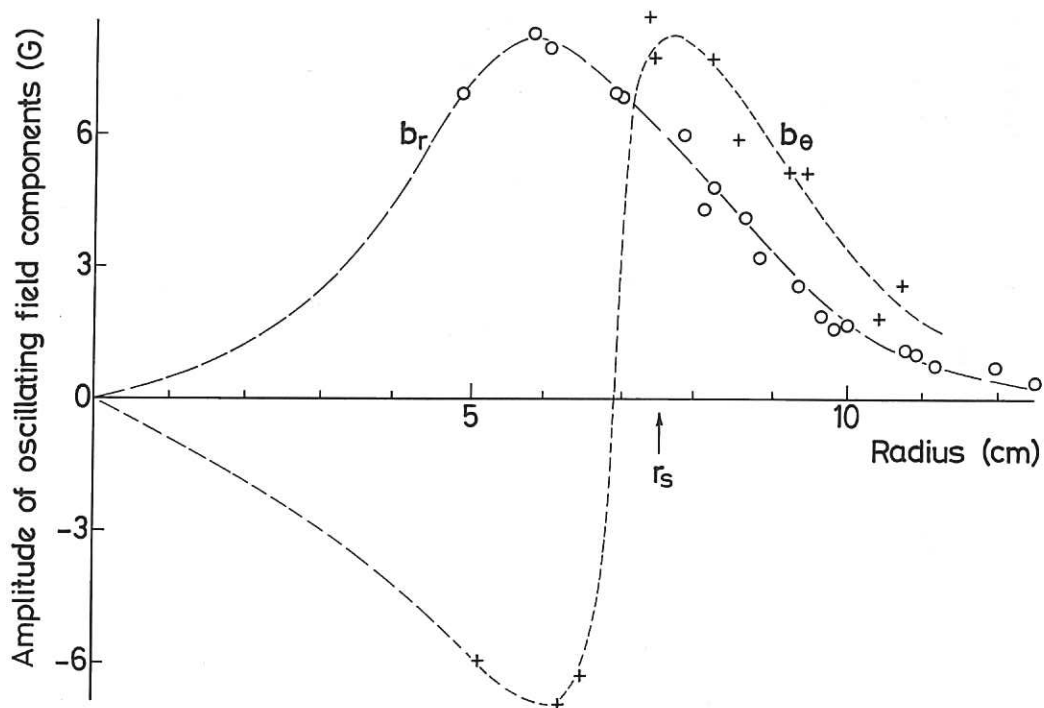


Fig. 2 Radial distribution of oscillating radial and poloidal field components. The radius at which $q=3$ is indicated by r_s .

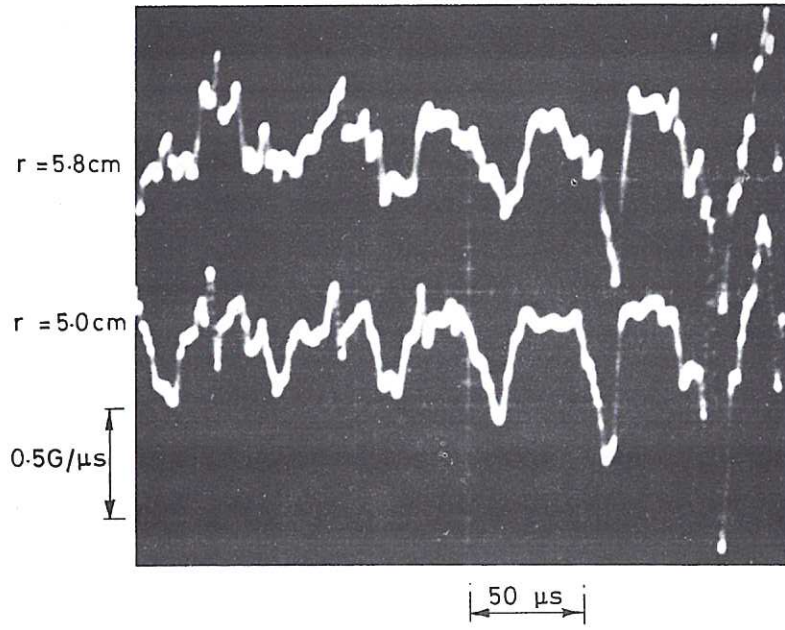


Fig.3 Time variation of the rate of change of radial field ($< 100 \text{ kHz}$) at two radial positions. Vertical scale $0.5 \text{ G}/\mu\text{s}$ /division, horizontal $50 \mu\text{s}$ /division.

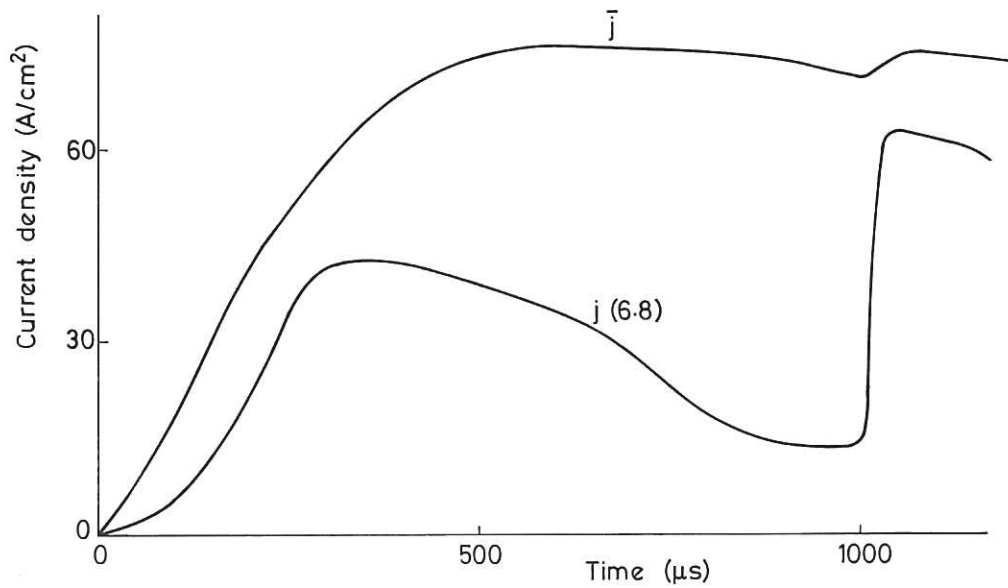


Fig.4 Evolution of the measured current density at a radius of 6.8 cm compared with the mean current density.

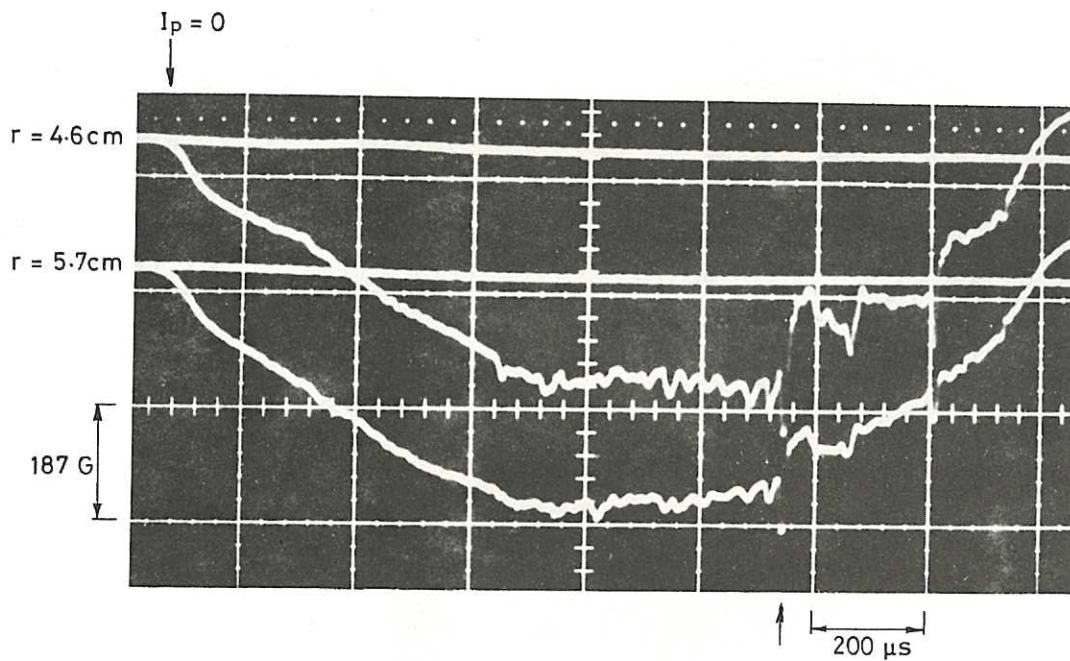


Fig. 5 Evolution of the poloidal field as measured at a radius of 4.6 cm and 5.7 cm showing the rise in amplitude of an $m=2$ instability leading to a disruption. Vertical scale 187 G/division, horizontal $200 \mu\text{s}$ /division.

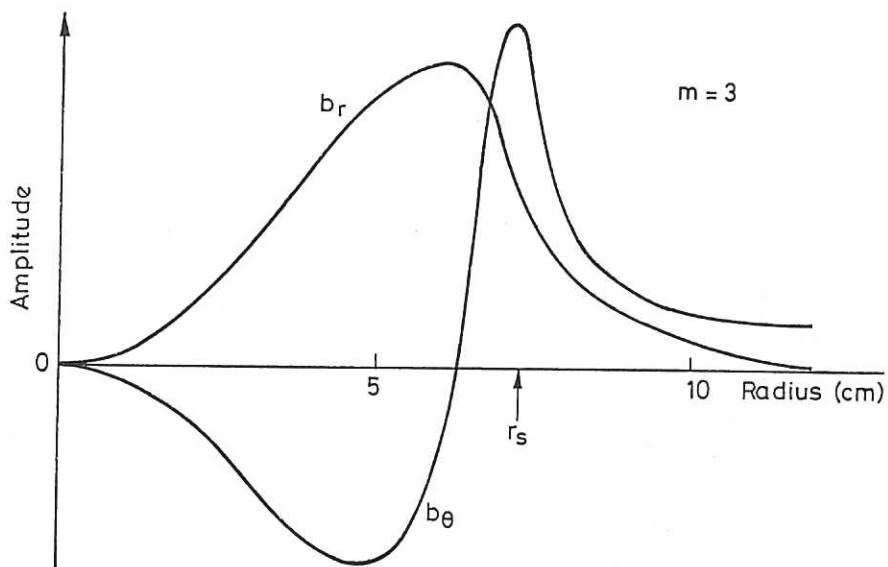


Fig. 6 Computed radial and poloidal field distributions for an $m=3$ tearing mode. The radius, r_s , at which $q=3$ is indicated. The magnetic Reynolds number with respect to the poloidal field was 1500.

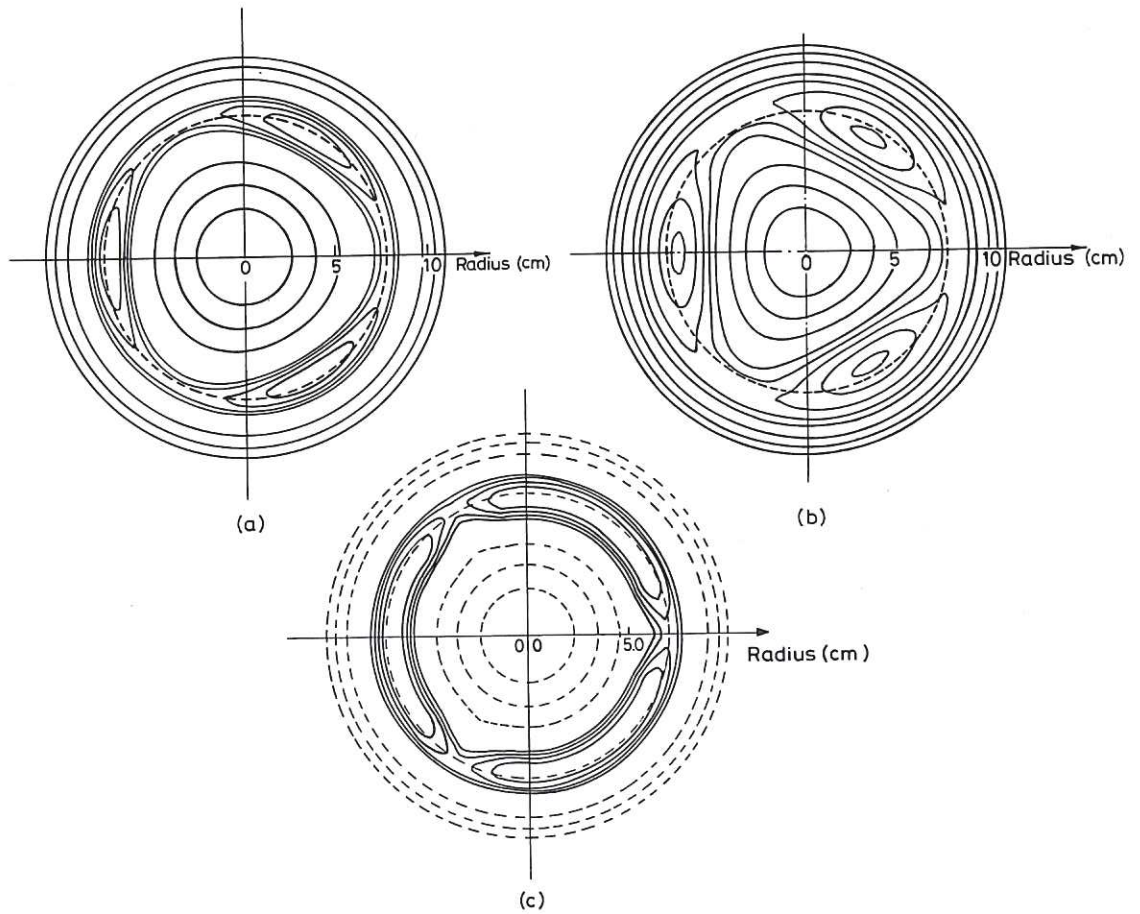


Fig.7 Computed flux contours for $m=3$ tearing mode with
 (a) $b_r/B_\theta = 1\%$
 (b) $b_r/B_\theta = 4\%$
 (c) $b_r/B_\theta = 1\%$ but with the observed time variation.

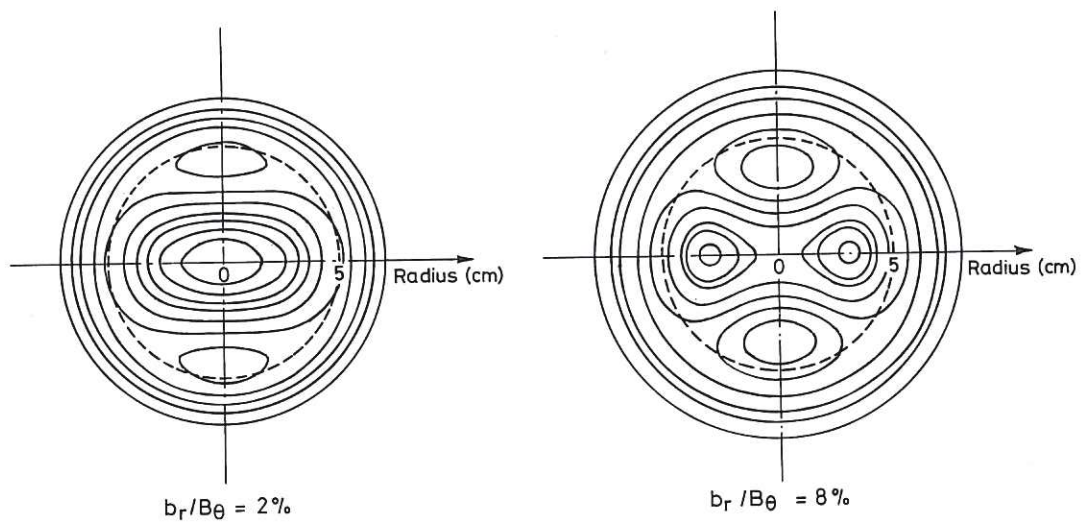


Fig.8 Computed flux contours for the $m=2$ tearing mode
 with amplitudes $b_r/B_\theta = 2$ and 8% .

The first part of the document discusses the importance of maintaining accurate records of all transactions. It emphasizes that every entry should be supported by a valid receipt or invoice. This not only helps in tracking expenses but also ensures compliance with tax regulations.

In the second section, the author provides a detailed breakdown of the company's revenue streams. This includes sales from various product lines and services. The data shows a steady increase in revenue over the past year, which is attributed to strategic marketing efforts and product diversification.

The third section focuses on the company's operational costs. It details the expenses related to manufacturing, distribution, and administrative functions. The analysis reveals that while some costs have increased due to inflation, others have been managed effectively through cost-cutting measures.

Finally, the document concludes with a summary of the overall financial performance. It highlights the company's strong financial health and its ability to generate consistent profits. The author expresses confidence in the company's future growth and success.

